Damage Classification of a Bolted Connection using Guided Waves and Explainable Artificial Intelligence

Hu, Muping; Yue, Nan; Groves, Roger M.

DOI
10.1016/j.prostr.2023.12.023

Publication date
2024

Document Version
Final published version

Published in
Procedia Structural Integrity

Available online at www.sciencedirect.com

ScienceDirect

Procedia Structural Integrity 52 (2024) 224–233

Structural Integrity Procedia

www.elsevier.com/locate/procedia

Fracture, Damage and Structural Health Monitoring

Damage Classification of a Bolted Connection using Guided Waves and Explainable Artificial Intelligence

Muping Hu[a,b,*], Nan Yue[b], Roger M. Groves[b]

[a]*College of Aerospace and Civil Engineering, Harbin Engineering University, Harbin 150001, P.R. China*
[b]*Aerospace Structures & Materials Department, Delft University of Technology, Delft 2629 HS, The Netherlands*

Abstract

With the improvements in computational power and advances in chip and sensor technology, the applications of machine learning (ML) technologies in structural health monitoring (SHM) are increasing rapidly. Compared with traditional methods, deep learning based SHM (Deep SHM) methods are more efficient and have a higher accuracy. However, due to the *black box* nature of deep learning, the trained models are usually difficult to interpret, which blocks their practical application. Therefore, it is of great importance to develop explainable artificial intelligence (XAI) methods to understand the internal decision-making mechanisms of damage classification in Deep SHM. In this paper, a novel XAI algorithm named Deep Gradient-weighted Class Activation Mapping (Deep Grad CAM) is proposed by combining the existing method Grad CAM with the convolutional neural network (CNN) deconvolution mechanism. In this paper, Deep Grad CAM is used to interpret a one-dimensional convolutional neural network trained to detect bolt loosening based on guided wave propagation. The interpretation performance of Deep Grad CAM is compared with Grad CAM, and their performances are quantified using Infidelity. The results show that the Infidelity of Deep Grad CAM is much smaller than that of Grad CAM, indicating significant improvements in explanation accuracy and reliability.

Keywords: guided waves; deep learning; explainable AI (XAI); one-dimensional convolutional neural network (1D CNN); structural health monitoring (SHM)

* Corresponding author. Tel.: +86 15546633132
E-mail address: humuping@hrbeu.edu.cn

2452-3216
10.1016/j.prostr.2023.12.023

1. Introduction

Bolted connections are widely used due to their low cost, convenient installation and disassembly (Wang et al. 2022). However, during their service life, bolts often undergo fatigue loads or corrosion, which can lead to the reduction of preload force and separation of the bolt connections. If bolt loosening cannot be detected in a timely manner, it may affect the structural integrity, reduce the load-bearing capacity and could ultimately lead to catastrophic accidents (Thoppul et al. 2009, Qin et al. 2022). Therefore, detecting the looseness of bolted joints is crucial for ensuring the safe operation of structures or components.

In recent decades, numerous new SHM methods for detecting bolt looseness have emerged, such as the electromechanical impedance method (Zhuang et al. 2018, Wang et al. 2021), fiber Bragg grating sensors (Ren et al. 2018, Yeager et al. 2018), guided wave-based methods (Fierro et al. 2018, Tola et al. 2020), and so on. However, these methods typically necessitate specialized high-precision instruments and dedicated post-processing software, which rely on manual operation by professionals. Large-scale bolt looseness detection relying on manual methods can be costly and time-consuming, particularly for extreme working conditions such as high temperature, high pressure, icing or strong winds. Therefore, there is a pressing need for efficient, accurate, and cost-effective automated SHM methods that are less reliant on human intervention.

As a breakthrough in artificial intelligence, deep learning (DL) can overcome the aforementioned problems. In recent years, many Deep SHM methods have been proposed (Yue et al. 2016, Abdeljaber et al. 2017, Azimi et al. 2020, Ma et al. 2021, Nokhbatolfoghahai et al. 2022, Cristiani et al. 2022, Hamishebahar et al. 2022, Pan et al. 2023, Zhang et al. 2023, Dang et al. 2023). Among them, CNN has received special attention due to its stronger generalization performance as the result of its deeper network structure. It can automatically process and learn the optimal features in raw data, achieving highly accurate classification without requiring data preprocessing (Tang et al. 2023). However, the complexity of CNN structures, and advanced AI algorithms in general, often makes their results challenging to explain and prove to humans. Clearly, an AI model's prediction accuracy on a finite data set does not guarantee its performance on (Ewald et al. 2022). This raises a critical question: in what way can human decision-makers trust the results of AI algorithms and prove their rationality?

This is why explainable artificial intelligence (XAI) is gaining popularity as a new field in machine learning (Bhakte et al. 2022, Al-Bashiti et al. 2022). XAI methods focus on interpreting the data processing operations performed by neural networks, enabling us to comprehend the underlying principles behind accurate model predictions(Meister et al. 2021). For a deep CNN, the convolutional layers often contain the most abundant spatial and semantic information, which is easier to interpret than the highly abstract information contained in fully connected layers. Therefore, Grad CAM (Selvaraju et al. 2019), which focuses on convolutional layer feature interpretation and has high generalization ability, is popular for explaining two-dimensional CNN (2D CNN).

However, Grad CAM may not acclimatize in a one-dimensional CNN (1D CNN) which is powerful in automatic feature extraction for processing long-length time series signals (Ince et al. 2016, Kiranyaz et al. 2021). In general, the important score vector obtained by Grad CAM needs to be mapped into the input space by linear interpolation. However, in 1D CNN, the dimensions of convolutional layers rapidly decrease. The linear mapping of Grad CAM result tends to assign high importance score over an extensive length of time series signal input, which might not be the accurate interpretation of 1D CNN.

Therefore, this paper proposes a new XAI method named Deep Grad CAM that takes into account the hierarchical structure of the CNN and utilizes a deconvolution mechanism for the backpropagation of explanation results. Specifically, a 1D CNN is trained using the monitored Lamb wave signals to detect bolt connections in a double-layer aluminum plate. Then, the model is interpreted using Grad CAM and Deep Grad CAM to investigate the reference basis for the model's decision-making process. The interpretability accuracy and reliability of the two algorithms are evaluated using the Infidelity.

2. Explainable artificial intelligence

2.1. Gradient-weighted Class Activation Mapping (Grad CAM)

Previous work has proven that convolutional layers naturally preserve spatial information lost in fully connected layers, making the features captured by them more easily understood from a physical perspective. Therefore, Selvaraju et al. (Selvaraju et al. 2019). proposed the Grad CAM algorithm for 2D CNN, which uses the gradient information flowing into the last convolutional layer of the CNN to assign importance values to each neuron in order to obtain specific interest decisions. Grad CAM can be used to evaluate the importance of each input signal in this work. The importance score vector of the *l*-th activation layer calculated from Grad CAM algorithm can be represented as:

$$I^l = ReLU\left(\sum_k \alpha_k^c A^k\right) \tag{1}$$

where *ReLU* is the activation function of rectified linear unit, *k* is the *k*-th channel, *c* represents the classes, A^k respects to the activation of the corresponding convolutional layer in channel *k*, and α_k^c is the weight of A^k which can be expressed as:

$$\alpha_k^c = \frac{1}{N}\sum_n \frac{\partial y^c}{\partial A_n^k} \tag{2}$$

where y^c represents the class score predicted by the model, A_n^k represents the *n*-th data of A^k, and *N* is the length of the activation layer.

In general, the important score vector obtained by Grad CAM needs to be mapped into the input space by linear interpolation, so the result of which is a coarse localization that represents where the model has to look to make the particular decision (Selvaraju et al. 2019). But in the application of 1D CNN in this paper, to avoid overfitting and high training costs due to excessive parameters, large kernel sizes and strides are set in the convolutional layers. As a result, the input vector undergoes rapid dimension reduction after each convolutional layer. In this case, the linearly mapping importance score vector back to the input space would require a significant dimensionality increase, which may result in an excessive area in the input vector being marked as important, thus affecting the accuracy of the explanation. Therefore, based on Grad CAM, the novel Deep Grad CAM algorithm proposed in this paper incorporates the hierarchical structure of 1D CNN convolutional layers to propagate the importance vector using its backpropagation mechanism instead of linear mapping.

2.2. Deep Gradient-weighted Class Activation Mapping (Deep Grad CAM)

To account for the limitation of the Grad CAM algorithm for 1D CNN, the backpropagation mechanism of the 1D CNN is used to propagate the importance score vector in the form of deconvolution to the input vector space in the Deep Grad CAM. Specifically, the *α*-*β* rule (Bach et al. 2015) is applied to propagate I^l layer by layer:

$$I_i^{l-1} = a_i \sum_j \frac{w_{ij}^+}{\sum_i a_i w_{ij}^+ + b_j^+} I_j^l \tag{3}$$

where I_i^{l-1} represents importance score of the *i*-th activation in ($l-1$)-th layer, I_j^l represents importance score of the *j*-th activation in *l*-th layer. a_i represents the activation value at the *i*-th point in the ($l-1$)-th layer. w_{ij}^+ and b_j^+ are the positive parts of the network weights and biases, respectively. By propagating I^l forward layer by layer, the importance score for the input vector can eventually be obtained.

2.3. Infidelity

Infidelity is defined as the expected difference between the two terms: (a) the dot product of the input perturbation to the explanation function and (b) the output perturbation. Therefore, it actually measures the consistency between model predictions and model explanations, and can be used to evaluate the reliability of XAI algorithms. Given a neural network function $\mathbf{f}$, explanation function Φ, the Gaussian perturbations R with probability measure μ_R, Infidelity can be expressed as:

$$\mathrm{INFD}(\Phi,\mathbf{f},\mathbf{x}) = \mathrm{E}_{R\sim\mu_R}\left[\left(R^T\Phi(\mathbf{f},\mathbf{x}) - (\mathbf{f}(\mathbf{x}) - \mathbf{f}(\mathbf{x}-R))\right)^2\right] \tag{4}$$

3. Numerical Simulation

3.1. Simulation model and Guided wave propagation

The propagation of Lamb waves in a double-layer aluminum plate was simulated using ABAQUS software. The Young's modulus of the aluminum plate is 71 *GPa*, density is 2700 kg/m^3, and Poisson's ratio is 0.33. Both layers of the aluminum plate are 2 *mm* thick and are in contact by using Tie. A schematic of the aluminum plate and transducer array is shown in Fig. 1. (a), with four 8 *mm* diameter piezoelectric sensors (PZT) placed on the aluminum plate. PZT1 was used as the excitation source, while the other three sensors acted as receivers. A steel bolt with a diameter of 6 *mm* was placed between PZT2 and PZT4, and the bolt hole on the plate is 6.6 *mm*. The Young's modulus of the bolt is 206 *GPa*, density is 7800 kg/m^3, and Poisson's ratio is 0.3. The propagation of Lamb waves in the plate was studied under both tightly connected and loosened conditions of the bolt. In the tightly connected case (Connected plate), the bolt and the aluminum plate were in contact by using Tie. In the loosened case (Damaged plate), the interactions between them are removed.

The numerical simulation model of the aluminums plate is shown in Fig. 1. (b). A concentrated force is applied at PZT1 to excite the Lamb wave, and the excitation signal is a tone burst of 3 cycles with a Hanning- window centered at 200 *kHz*, which is symmetrically loaded along the thickness direction of the plate. The Lamb waves excited by this signal only contain the S_0 mode. As the shortest wavelength of the S_0 mode Lamb wave at 200 *kHz* is 15.55 *mm*, the mesh size was set to 1 *mm*. The element type is the eight-node brick element with reduced integration (C3D8R), with a total of 641,528 elements. The time increment step was set to 0.01 μs, the sampling frequency is 10 *MHz*, and the recorded time length was 0.12 *ms*. The explicit dynamics solver was used.

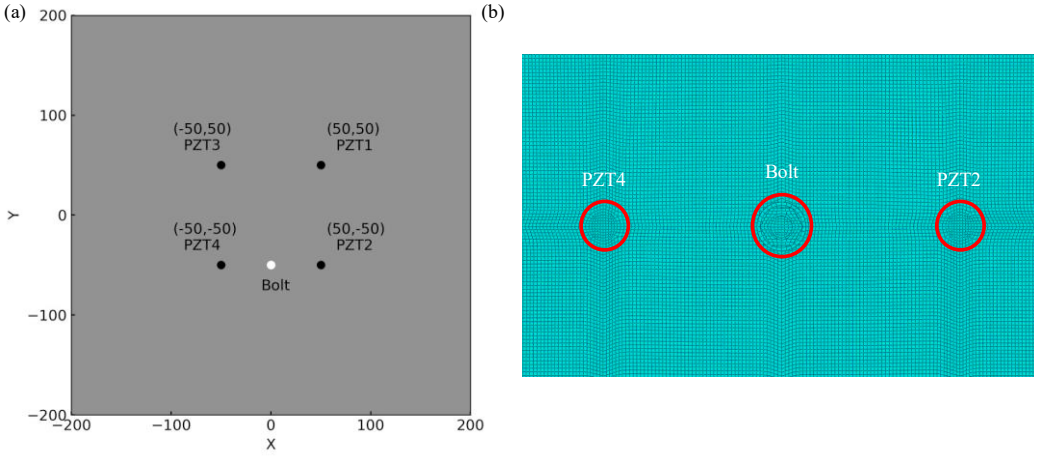

Fig. 1. (a) Schematic of the aluminum plate and transducer array; (b) Simulation model of the bolted plate

The propagation of Lamb waves in the Connected plate and Damaged plate are shown in Fig. 2 and Fig. 3, respectively. It can be seen that when the aluminum plate and bolt are tightly connected, there are clear reflection when the Lamb waves reach the bolt, and some of the Lamb waves become trapped in the bolt and continue to reflect inside it before spreading outwards. Therefore, the bolt becomes a weak secondary excitation source where a sustained excitation phenomena can be observed. In the case of the Damaged plate, there is no connection between the bolt and the aluminum plate, an obvious reflection of Lamb waves can be observed at the periphery of bolt hole, but the Lamb waves cannot propagate inside the bolt, so the phenomenon of sustained secondary excitation disappears. It can be seen from the comparison that the reflection phenomenon is more complex in the case of the tightly connected plate, because in addition to the reflection at the bolt hole, there are also reflection waves from inside the bolt.

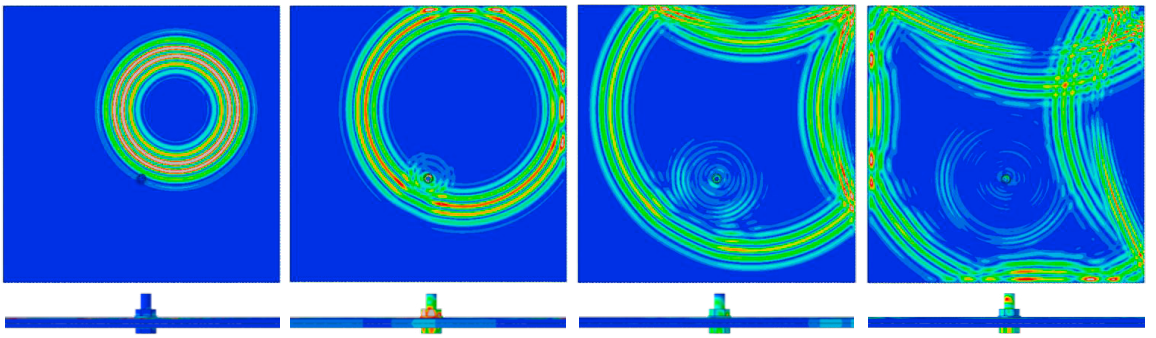

Fig. 2. Propagation of Lamb waves in the Connected plate: (a) $2.4 \times 10^{-5}\,s$; (b) $3.6 \times 10^{-5}\,s$; (c) $4.8 \times 10^{-5}\,s$; (d) $6.0 \times 10^{-5}\,s$

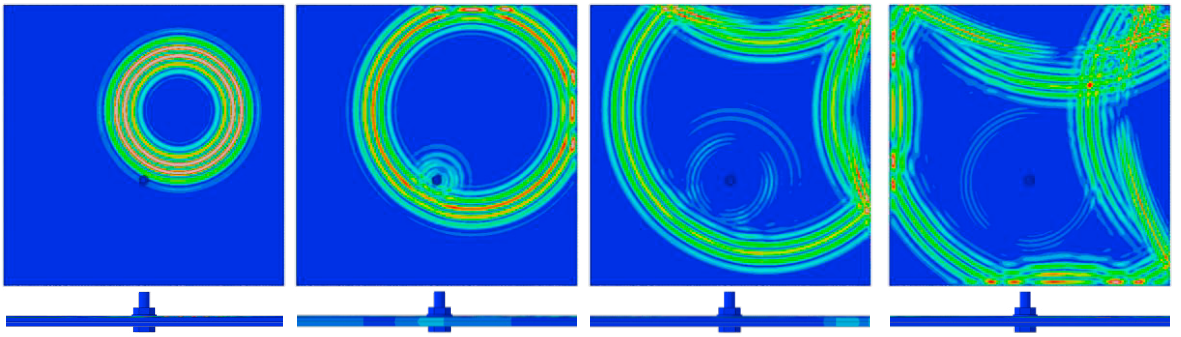

Fig. 3. Propagation of Lamb waves in the Damaged plate: (a) $2.4 \times 10^{-5}\,s$; (b) $3.6 \times 10^{-5}\,s$; (c) $4.8 \times 10^{-5}\,s$; (d) $6.0 \times 10^{-5}\,s$

3.2. Signal analysis and CNN architecture

Excitation was applied at PZT1 on the Connected and Damaged plates, and signals were received at PZT2, PZT3, and PZT4, with a signal length of 1200 samples. Then, 200 sets of Gaussian white noise are added to each signal to simulate experimental noise. The signal-to-noise ratio (SNR) after adding white noise is 20 *dB*. The definition of SNR is:

$$SNR(dB) = 10\log_{10}\left(P_{signal} \,/\, P_{noise}\right) \tag{5}$$

where $P_{signal}=\frac{1}{n}\sum_{i=1}^{n}s_i^2$, $P_{noise}=\frac{1}{n}\sum_{i=1}^{n}w_i^2$ and $S\sim(s_1,s_2\cdots s_n)$ is the raw signal, $W\sim(w_1,w_2\cdots w_n)$ is the white noise signal.

The noisy signals are utilized to build the training and testing sets for 1D CNN. As shown in Fig. 4, the signals received by PZT2, PZT3, and PZT4 are concatenated end-to-end to form a new one-dimensional vector of length 3600, which serves as the input of 1D CNN. The residual signal is the difference between the signals received from the Connected plate and the Damaged plate. As can be seen from the figure, each individual signal consists of three parts: direct wave, bolt reflection wave (Bolt R) or hole reflection wave (Hole R), and boundary reflection wave. The law reflected in the signals is consistent with that in the wave propagation diagram in section 3.1: the bolt reflection wave is more complex than the hole reflection wave, with a larger amplitude and more wave packets. And it can be inferred from the residual signal that besides the differences caused by the bolt and hole reflection, there are also significant differences in the boundary reflection wave between the two signal groups.

The signals were used for binary classification by the 1D CNN, with a label of 0 representing a securely connected bolt and plate, and a label of 1 representing a loosened bolt. The size of the training set is 200 × 3600, with 200 samples in total, 100 sets of samples from the Connected plate and 100 sets of samples from the Damaged plate, and each input vector has a length of 3600. The size of the testing set is 200 × 3600. The CNN model has eight layers, including one input layer, three convolutional layers, three fully connected layers, and one output layer. The input layer has a size of 3600. The output channels of the convolutional layers are set to 64, 128, and 256, with kernel sizes of 40, 20, and 10, a stride of 2, and a pooling layer size of 2. The three fully connected layers have 2048, 512, and 128 neurons, respectively, and use Rectified Linear Unit (*ReLU*) as the activation function. The length of the output layer is 2.

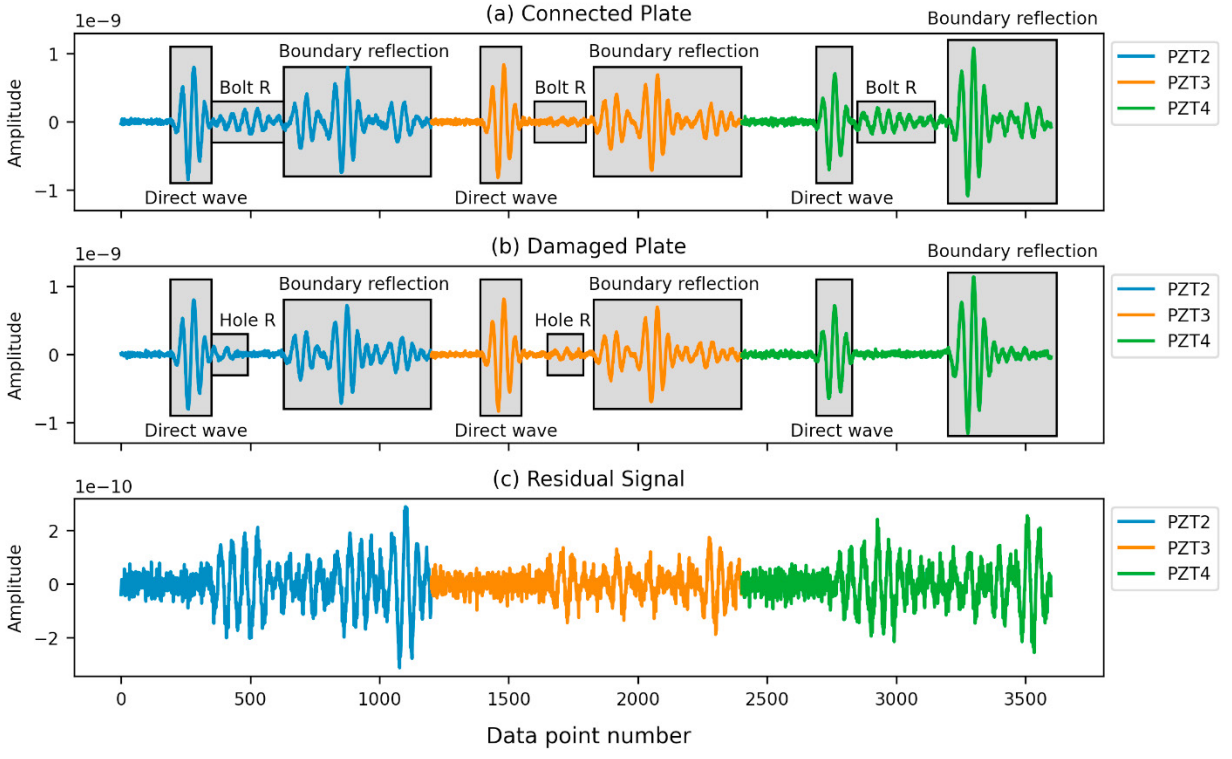

Fig. 4. Received signals by PZT2, PZT3 and PZT4 (a) from Connected Plate (b) from Damage Plate and (c) Residual signal between the Connected and Damage Plate

4. Explanation of CNN

4.1. X AI result

The 1D CNN achieves a testing accuracy of 100%. Then, Grad CAM and Deep Grad CAM are used for explainable analysis of the well-trained model. Fig. 5 displays the result of importance scores of these two algorithms in the form of saliency map, where the regions closer to red indicate higher importance to the 1D CNN's decision, while closer to blue indicate lower importance. For the results of Grad CAM, almost all information in the signal is considered important as the signal is colored from start to end. Specifically, for Class 0, Grad CAM considers the boundary reflection wave in PZT2 and PZT4 and the direct wave in PZT4 to be the most important for CNN decision-making. The pattern of Class 1 is very similar to that of Class 0, the red regions appear in the direct wave and boundary reflection wave of PZT2 and PZT4. But it can also be observed that for both classes, a large portion of the high-score regions are distributed in the flat sections of the signal that are considered to not carry useful information.

The results of Deep Grad CAM are more concentrated than those of Gram CAM. For Class 0, the high-score regions identified by Deep Grad CAM coincide very well with the regions of large absolute residual signal values, and the algorithm considers the bolt and boundary reflection wave received by PZT2 and PZT4 to be very important, which is consistent with the logic of signal analysis because signals received by PZT2 and PZT4 have greater differences on the Connected and Damaged plates. But the direct wave of PZT3 and PZT4 is also considered important. For Class 1, Deep Grad CAM suggests that 1D CNN relies more on the signals from PZT3 and PZT4 for classification and considers direct waves more important, which is very different from Class 0. From the above comparison, it can be seen that the results of Deep Grad CAM are easier to understand because its colored regions are concentrated on the location of wave packets, and the high-score regions identified by it have a higher degree of coincidence with the residual signal, which is more consistent with human expert knowledge of SHM.

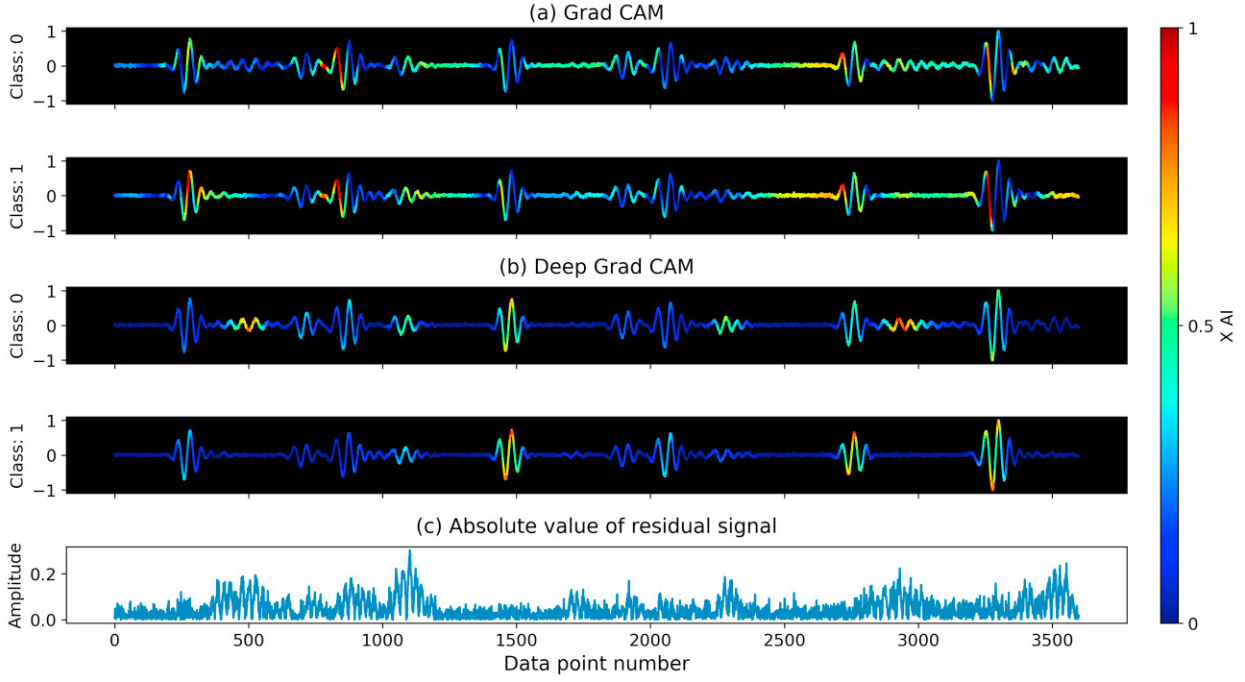

Fig. 5. Example of the importance score for the signals from class 0 and 1 (a) Analyzed by Grad CAM (b) Analyzed by Deep Grad CAM and (c) Absolute value of residual signal between class 0 and class 1.

Fig. 6 compares the Infidelity of Grad CAM and Deep Grad CAM for two classes. A smaller Infidelity value indicates a closer model prediction and model explanations, and the higher the reliability of the XAI. As shown in the figure, both XAI algorithms exhibit lower Infidelity on Class 1, which means both them have a better performance on

the explanation for the classification of the signals from Class 1. The signals from class 0 are more complex, carrying more bolt reflection information. Therefore, it can be inferred that when the data to be explained is more complex, the uncertainty of the model explanation also increases. Furthermore, on both classes, the Infidelity of Deep Grad CAM is much lower than that of Grad CAM, indicating that the former provides more accurate explanations of the CNN model and its reliability is significantly higher.

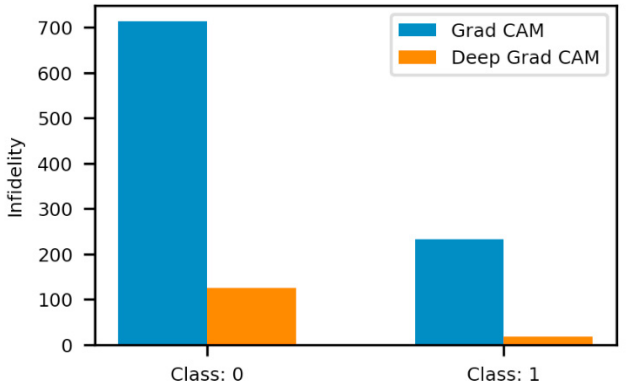

Fig. 6. The Infidelity results of Grad CAM and Deep Grad CAM on testing database

5. Conclusions

This paper numerically analyses the propagation of guided waves in bolted connection plates, classifies bolt connections using 1D CNN, and then uses Deep Grad CAM and Grad CAM to analyze the main reference features of CNN during classification in the form of saliency maps. The performance of the two XAI algorithms was evaluated using Infidelity, and the following conclusions are drawn:

1. Bolt reflection is more complex than hole reflection. The wave propagation and signal analysis diagrams show that a bolt, when tightly connected to a plate, becomes a secondary excitation source during the propagation of Lamb waves. The Lamb waves continue to reflect inside the bolt and spread outward, resulting in received bolt reflection waves having more wave packets and complex modes.

2. Deep Grad CAM's importance score results are more consistent with the analysis logic of SHM. The saliency map shows that the high-score region of Deep Grad CAM matches the peak region of the residual signal better. Such a high degree of agreement indicates that Deep Grad CAM considers that 1D CNN, like humans, pays more attention to the parts with greater differences between two contrasting signals.

3. Deep Grad CAM is more reliable. Infidelity comparison results reveal that the Infidelity of both damage classes of Deep Grad CAM is far smaller than that of Grad CAM. Which means that the explanation of Deep Grad CAM is closer to the prediction of the CNN model, and therefore its accuracy is higher.

6. Acknowledgement

This research is part of the European Union Horizon Europe OVERLEAF project and is supported under grant agreement No. 101056818.

References

Abdeljaber, O., O. Avci, S. Kiranyaz, M. Gabbouj & D. J. Inman 2017. Real-time vibration-based structural damage detection using one-dimensional convolutional neural networks. Journal of Sound and Vibration, 388**,** 154-170.

Al-Bashiti, M. K. & M. Z. Naser 2022. Verifying domain knowledge and theories on Fire-induced spalling of concrete through eXplainable artificial intelligence. Construction and Building Materials, 348**,** 128648.

Azimi, M. & G. Pekcan 2020. Structural health monitoring using extremely compressed data through deep learning. Computer-Aided Civil and Infrastructure Engineering, 35**,** 597-614.

Bach, S., A. Binder, G. Montavon, F. Klauschen, K. R. Muller & W. Samek 2015. On Pixel-Wise Explanations for Non-Linear Classifier Decisions by Layer-Wise Relevance Propagation. Plos One, 10.

Bhakte, A., V. Pakkiriswamy & R. Srinivasan 2022. An explainable artificial intelligence based approach for interpretation of fault classification results from deep neural networks. Chemical Engineering Science, 250**,** 117373.

Cristiani, D., F. Falcetelli, N. Yue, C. Sbarufatti, R. Di Sante, D. Zarouchas & M. Giglio 2022. Strain-based delamination prediction in fatigue loaded CFRP coupon specimens by deep learning and static loading data. Composites Part B: Engineering, 241.

Dang, V.-H., K. Le-Nguyen & T.-T. Nguyen 2023. Semi-supervised vibration-based structural health monitoring via deep graph learning and contrastive learning. Structures, 51**,** 158-170.

Ewald, V., R. Sridaran Venkat, A. Asokkumar, R. Benedictus, C. Boller & R. M. Groves 2022. Perception modelling by invariant representation of deep learning for automated structural diagnostic in aircraft maintenance: A study case using DeepSHM. Mechanical Systems and Signal Processing, 165**,** 108153.

Fierro, G. P. M. & M. Meo 2018. IWSHM 2017: Structural health monitoring of the loosening in a multi-bolt structure using linear and modulated nonlinear ultrasound acoustic moments approach. Structural Health Monitoring-an International Journal, 17**,** 1349-1364.

Hamishebahar, Y., H. Guan, S. P. So & J. Jo 2022. A Comprehensive Review of Deep Learning-Based Crack Detection Approaches. Applied Sciences-Basel, 12.

Ince, T., S. Kiranyaz, L. Eren, M. Askar & M. Gabbouj 2016. Real-Time Motor Fault Detection by 1-D Convolutional Neural Networks. IEEE Transactions on Industrial Electronics, 63**,** 7067-7075.

Kiranyaz, S., O. Avci, O. Abdeljaber, T. Ince, M. Gabbouj & D. J. Inman 2021. 1D convolutional neural networks and applications: A survey. Mechanical Systems and Signal Processing, 151.

Ma, D. L. & D. Y. Wang 2021. A deep learning-based method for hull stiffened plate crack detection. Proceedings of the Institution of Mechanical Engineers Part M-Journal of Engineering for the Maritime Environment, 235**,** 570-585.

Meister, S., M. Wermes, J. Stuve & R. M. Groves 2021. Investigations on Explainable Artificial Intelligence methods for the deep learning classification of fibre layup defect in the automated composite manufacturing. Composites Part B-Engineering, 224.

Nokhbatolfoghahai, A., H. M. Navazi & R. M. Groves 2022. Use of dictionary learning for damage localization in complex structures. Mechanical Systems and Signal Processing, 180.

Pan, X. & T. Y. Yang 2023. 3D vision-based bolt loosening assessment using photogrammetry, deep neural networks, and 3D point-cloud processing. Journal of Building Engineering, 70**,** 106326.

Qin, X., C. Peng, G. Zhao, Z. Ju, S. Lv, M. Jiang, Q. Sui & L. Jia 2022. Full life-cycle monitoring and earlier warning for bolt joint loosening using modified vibro-acoustic modulation. Mechanical Systems and Signal Processing, 162**,** 108054.

Ren, L., T. Feng, M. Ho, T. Jiang & G. Song 2018. A smart “shear sensing” bolt based on FBG sensors. Measurement, 122**,** 240-246.

Selvaraju, R. R., M. Cogswell, A. Das, R. Vedantam, D. Parikh & D. Batra 2019. Grad-CAM: Visual Explanations from Deep Networks via Gradient-Based Localization. International Journal of Computer Vision, 128**,** 336-359.

Tang, R., S. Zhang, W. Wu, S. Zhang & Z. Han 2023. Explainable deep learning based ultrasonic guided wave pipe crack identification method. Measurement, 206**,** 112277.

Thoppul, S. D., J. Finegan & R. F. Gibson 2009. Mechanics of mechanically fastened joints in polymer–matrix composite structures – A review. Composites Science and Technology, 69**,** 301-329.

Tola, K. D., C. Lee, J. Park, J. W. Kim & S. Park 2020. Bolt looseness detection based on ultrasonic wavefield energy analysis using an Nd:YAG pulsed laser scanning system. Structural Control and Health Monitoring, 27.

Wang, F. & G. Song 2021. A novel percussion-based method for multi-bolt looseness detection using one-dimensional memory augmented convolutional long short-term memory networks. Mechanical Systems and Signal Processing, 161**,** 107955.

Wang, L., B. Yuan, Z. Xu & Q. Sun 2022. Synchronous detection of bolts looseness position and degree based on fusing electro-mechanical impedance. Mechanical Systems and Signal Processing, 174**,** 109068.

Yeager, M., A. Whitaker & M. Todd 2018. A method for monitoring bolt torque in a composite connection using an embedded fiber Bragg grating sensor. Journal of Intelligent Material Systems and Structures, 29**,** 335-344.

Yue, N., Z. S. Khodaei & M. H. Aliabadi. 2016. Passive sensing of sensorized composite panels: Support vector machine. In Key Engineering Materials, 199-202.

Zhang, S., H. Lei, Z. Zhou, G. Wang & B. Qiu 2023. Fatigue life analysis of high-strength bolts based on machine learning method and SHapley Additive exPlanations (SHAP) approach. Structures, 51**,** 275-287.

Zhuang, Y. T., F. Kopsaftopoulos, R. Dugnani & F. K. Chang 2018. Integrity monitoring of adhesively bonded joints via an electromechanical impedance-based approach. Structural Health Monitoring-an International Journal, 17**,** 1031-1045.